Shedding light on human cerebral lipofuscin

Received: 17 January 2020 | Revised: 12 June 2020 | Accepted: 21 June 2020

DOI: 10.1002/cne.24971

RESEARCH ARTICLE

JCN THE JOURNAL OF COMPARATIVE NEUROLOGY | WILEY

Shedding light on human cerebral lipofuscin: An explorative study on identification and quantification

Karlijn Hakvoort[1] | Louise Otto[2] | Roel Haeren[3,4] | Govert Hoogland[3,5] | Olaf Schijns[3,5] | Hans Vink[6] | Dionne Klein[7] | Marc van Zandvoort[8] | Kim Rijkers[3,5]

[1]Department of Neurosurgery, RWTH Aachen University, Aachen, Germany

[2]Department of Neurology, University Medical Center Utrecht, Brain Center Utrecht University, Utrecht, The Netherlands

[3]Department of Neurosurgery, School for Mental Health and Neuroscience, Maastricht University Medical Center+, Maastricht, The Netherlands

[4]Department of Neurosurgery, Helsinki University Central Hospital, Helsinki University, Helsinki, Finland

[5]Academic Center for Epileptology, Maastricht University Medical Center+ and Kempenhaeghe, Maastricht, The Netherlands

[6]Department of Physiology, School for Cardiovascular Diseases, CARIM, Maastricht University Medical Center+, Maastricht, The Netherlands

[7]Institute for Molecular Cardiovascular Research IMCAR, RWTH Aachen University, Aachen, Germany

[8]Department of Molecular Cell Biology, School for Mental Health and Neuroscience (MHeNS) and School for Cardiovascular Diseases (CARIM), Maastricht University Medical Center+, Maastricht, The Netherlands

Correspondence
Kim Rijkers, Department of Neurosurgery, School for Mental Health and Neuroscience, Maastricht University, Maastricht, Limburg, The Netherlands.
Email: kim.rijkers@mumc.nl

Abstract

Increased oxidative stress has been associated with several neurodegenerative diseases such as Alzheimer's disease, but also with neurological diseases sharing pathophysiological pathways like epilepsy. Lipofuscin is a nondegradable end-product of oxidative stress; its cerebral presence reflects the cumulative amount of oxidative stress the brain has endured. In this study, we have observed prominent autofluorescent particles in the pial arterial wall and in neocortical parenchyma of young, drug-resistant epilepsy patients (18–28 years old) who underwent resective brain surgery (n = 6), as well as in older control patients (n = 3). With fluorescence spectroscopic imaging, brightfield microscopy, histochemistry and fluorescence lifetime imaging, these autofluorescent particles were identified as the *age pigment* lipofuscin. An evaluation of these lipofuscin particles using Imaris© software allowed robust quantification, while the 3D properties allowed visualization of the complex configuration. We elaborate on the usefulness of lipofuscin as a marker of cumulative oxidative stress in the brain. Furthermore, we speculate on the observed differences in particle size and density that we found between young patients and older controls, which could imply a role for lipofuscin in the pathophysiology of epilepsy and possibly other neurological diseases.

KEYWORDS

biomarker, epilepsy, Imaris, RRID:SCR_007370, lipofuscin, oxidative stress, quantification

1 | INTRODUCTION

Lipofuscin is a nondegradable substance composed of lipids, proteins, carbohydrates and metals (Brunk & Terman, 2002; Al Terman & Brunk, 1998; Alexei Terman & Brunk, 2004). It is mainly found in lysosomes or within the cytosol. Formation of lipofuscin has been related to several cellular mechanisms, all associated with aging (Moreno-García, Kun, Calero, Medina, & Calero, 2018). These mechanisms include ineffective cellular proteostasis, altered lipid metabolism, and dysfunctional endolysosomal and mitochondrial pathways (Moreno-García et al., 2018). These mechanisms are all interconnected, and an increase in oxidative stress seems to play a major role in this interplay. Oxidative stress is a condition characterized by high metabolic activity with excessive generation of reactive oxygen

Karlijn Hakvoort and Louise Otto shared first author, both authors contributed equally to this work

Marc van Zandvoort and Kim Rijkers shared last author.

species that cannot be counterbalanced by the antioxidant defense system. It induces structural cell damage and facilitates aldehyde-mediated cross-linking of macro-molecules while they are being degraded in lysosomes, forming lipofuscin (Czerska, Mikołajewska, Zieliński, Gromadzińska, & Wąsowicz, 2015; Lushchak, 2014; Sies, 1997; Al Terman & Brunk, 1998). Due to its nondegradable nature, lipofuscin accumulates with time. The total amount of lipofuscin is indicative of the total amount of oxidative stress endured by the tissue over time (Brunk & Terman, 2002; Strehler, Mark, Mildvan, & Gee, 1959). It is therefore increasingly present with increasing age; hence, lipofuscin is often referred to as *age pigment*.

Pathological aging, for instance in neurodegenerative diseases such as Alzheimer's disease, is associated with increased oxidative stress compared to "physiological aging" (Islam, 2017; Lin & Beal, 2006; Pearson-Smith & Patel, 2017; Uttarra, Singh, Zamboni, & Mahajan, 2009). As such, neurodegenerative diseases have been associated with abnormal cerebral lipofuscin accumulation (Moreno-García et al., 2018). Importantly, recent insights in lipofuscin formation suggest that lipofuscin is likely to promote further oxidation. It is therefore considered as active mediator in formation of oxidative stress and could play a causal role in neurodegenerative processes, instead of solely being an inert by-product of oxidative stress (Brunk & Terman, 2002). Important features of neurodegeneration are often associated with vascular pathophysiology, including microvascular dysfunction, increased blood–brain barrier permeability, angiogenesis, and dysfunctional neurovascular coupling (Brown & Thore, 2011; Heinemann, Kaufer, & Friedman, 2012; Iadecola, 2004; Marchi & Lerner-Natoli, 2013; Parfenova et al., 2005; Rigau et al., 2007; E. A. van Vliet, Aronica, & Gorter, 2015). These vascular pathophysiological pathways have also been described in epilepsy (Heinemann et al., 2012; Marchi et al., 2009; Parfenova et al., 2005; Rigau et al., 2007; E. A. van Vliet et al., 2015). Indeed, increased levels of oxidative stress in brain tissue from epilepsy patients have been reported, suggesting a common vascular pathophysiological pathway related to oxidative stress in epilepsy (Aguiar et al., 2012; Chang & Yu, 2010; Puttachary, Sharma, Stark, & Thippeswamy, 2015; Rumià et al., 2013).

Microscopically, lipofuscin can quite easily be visualized and distinguished from other lipopigments, based on its specific autofluorescent properties (Collins, Arborgh, Brunk, & Schellens, 1980; Jung, Höhn, & Grune, 2010; Tohma, Hepworth, Shavlakadze, Grounds, & Arthur, 2011). Subsequent quantification is, however, challenging, because of the particles' irregular appearance and density.

In this study, we describe the analysis of autofluorescent particles encountered within the wall of pial arteries and within neocortical parenchyma, isolated from brain tissue obtained during resective brain surgery in epilepsy patients and nonepileptic/nonneurologically affected controls. These particles were identified as lipofuscin, and subsequently quantified using a novel developed method that allowed quantification in three dimensions. This study thus serves as a proof of concept of a novel 3D quantification method for lipofuscin, making use of a combined advanced microscopy technique. With this study we aim to contribute to further exploration of lipofuscin formation in relation to neurological diseases, in particular chronic epilepsy. Doing so, more insight in protein aggregation can be obtained, as this seems to be of importance in various neurodegenerative diseases and possibly also other neurological diseases like epilepsy.

2 | MATERIALS AND METHODS

2.1 | Materials

Brain tissue samples of six patients suffering from drug-resistant epilepsy were included (E1-E6, further referred to as patients). These samples were considered representative of a neurological disease featured by oxidative stress (Pauletti et al., 2019; Pearson-Smith & Patel, 2017). Samples were obtained during resective brain surgery, a treatment option for a selected group of drug-resistant epilepsy patients. Resected brain tissue was partly used for routine histopathological evaluation. Remaining tissue, that otherwise would have been discarded, was included for this study. Although no medical ethical approval was lawfully required, a preoperatively signed informed consent was obtained in all cases. Experimental protocols of human tissue-handling were in accordance with Good Clinical Practice guidelines.

Neocortical tissue obtained during resection of a high grade glioma in one patient (C1), as well as postmortem neocortical tissue obtained during autopsy in two patients (C2 and C3) were included as control samples. In the postmortem controls there was no history of neurological disorder. Demographic characteristics of patients and controls are summarized in Table 1.

Neocortical samples were subsequently processed using various imaging techniques, including histochemistry, fluorescence microscopy with brightfield microscopy (combined with Nuance software), two-photon laser scanning microscopy (TPLSM) and fluorescence lifetime imaging. Additionally, TPLSM was used to assess isolated pial arteries in a subset of patients, to evaluate lipofuscin quantity and distribution in a 3D structure. All techniques are elaborated on in this section.

2.2 | Tissue processing

Intraoperatively collected brain tissue samples of all patients (E1–E6) consisted of anterior temporal lobe neocortex. One part of the neocortex was immediately stored in HEPES-buffered physiologic salt solution (HEPES-PSS). HEPES-PSS was continuously maintained at a temperature of 37°C and contained in mM: KCl 4.7, NaCl 144, $CaCl_2$ 2.5, KH_2PO_4 1.2, $MgSO_4$ 1.2, HEPES 14.9, and glucose 5.5, pH 7.4. Subsequently, pial arteries of E1–E4 were isolated by microdissection, after which experiments were performed within 2–3 hr after resection.

Another part of the tissue was fixated in 4% paraformaldehyde for 48 hr, and subsequently embedded in paraffin and sectioned at a thickness of 8 μm. In one patient (E1), an additional part of the collected tissue was stored as fresh-frozen tissue at minus 80°C directly following resection and sectioned at a thickness of 12 μm.

TABLE 1 Demographic characteristics

	Epilepsy patients						Control group		
	E1	E2	E3	E4	E5	E6	C1	C2	C3
Sex	M	F	M	F	M	M	M	F	M
Age (years)	23	19	18	28	28	19	61	53	39
Epilepsy duration (years)	17	11	17	12	14	6	n/a	n/a	n/a
Tissue origin[a]	ATL + AH	ATL + AH	Hemisphe-rotomy	ATL + AH	ATL + AH	ATL + AH	Debulking high grade glioma	Autopsy	Autopsy
Cause of death	n/a	n/a	n/a	n/a	n/a	n/a	n/a	Unknown, not neuro-logical	Cardiac arrest
TPLSM[b] analysis in pial artery + quantification	×	×	×	×			×		
Fluorescence spectroscopic imaging	×	×			×	×		×	×
Autofluores-cence lifetime analysis	×								
Histochemistry		×			×	×		×	×

Note: Demographic details of the included patients and controls are presented. Most of the patient tissue has been derived during surgery (ATL + AH) for temporal lobe epilepsy. Cause of death is also included for the postmortem tissue (C2–C3). In the lower rows of the table, we have indicated the experiments in which the tissue was included.

[a]ATL + AH = anterior temporal lobectomy and amygdalohippocampectomy.

[b]TPLSM = two-photon laser scanning microscopy.

Postmortem material was obtained within 72 hr after death and fixated in 4% paraformaldehyde for 48 hr, subsequently embedded in paraffin and sectioned at 8 μm thickness.

2.3 | Fluorescence spectroscopic imaging

Unstained paraffin sections of neocortical samples of four patients (E1, E2, E5, E6) and two controls (C1, C2) were used for autofluorescence spectrum analysis. A Leica DM4000 B LED microscope (Leica Microsystems GmbH, Wetzlar, Germany) was used with HC PLAN APO ×20/0.70 and HC PLAN APO ×40/0.75 water objectives, and an HXC PLAN APO ×100/1.40–0.70 oil immersion objective. Images were recorded using a Nuance Multispectral Imaging System (PerkinElmer, Hopkinton, MA) with version 3.0.2 software.

Nuance microscopy registers the spectrum of light emitted by a specimen when excited in a narrow wavelength range. We applied excitation wavelengths between 420 and 460 nm, while emission was evaluated through a long pass filter, passing all fluorescence above 420 nm. The spectrum, obtained in ascending steps of 20 nm, was determined from several autofluorescent particles located in both the pial artery vascular wall and the neocortical tissue sections. Subsequently, multispectral analysis was performed by "unmixing" the generated spectral curves of the various fluorescent materials, thereby differentiating the spectrum of the particles of interest from the spectrum of other (background) structures. To assess potential influence of formaldehyde and/or paraffin on the spectrum, the analysis was repeated on fresh-frozen tissue in one patient (E1).

2.4 | Brightfield microscopy and histochemistry

Periodic acid Schiff's (PAS) staining was performed on neocortical slides adjacent to the slides used for fluorescence microscopy of patients (E2, E5, E6) and controls (C1, C2). Schiff's reagent detects polysaccharides, an important component of lipofuscin. Neocortical slides were first deparaffinized and treated with periodic acid 0.5% solution for 5 min, then rinsed with distilled water. Subsequently, slides were put in Schiff's reagent for 15 min and washed in tap water for 5 min. Hereafter, slides were mounted and analyzed with Brightfield microscopy (BX51TF, Olympus) at 20 and 40 times magnification.

2.5 | Fluorescence lifetime imaging

Additional autofluorescent characteristics of the particles were obtained by performing lifetime analysis using fluorescence lifetime imaging measurement. First, autofluorescence spectrum measurement was repeated to verify the analysis of similar autofluorescent particles, using a Leica TCS SP5 two-photon laser scanning microscope (Microsystems GmbH, Wetzlar, Germany) with the settings described below.

Fluorescence lifetime imaging was then performed with a Becker and Hickl time correlated single photon counting module (SPC 830, Becker & Hickl, Berlin, Germany). Three de-scanned color-coded PMT detectors were used for detection, namely 400–420 nm (blue), 429–513 nm (green), and 518–646 nm (red).

Obtained lifetime images were analyzed using a bi-exponential decay curve. Mean lifetime was calculated using the following formula: $\tau_{mean} = (\alpha_1 \bullet \tau_1^2 + \alpha_2 \bullet \tau_2^2) / (\alpha_1 \bullet \tau_1 + \alpha_2 \bullet \tau_2)$ [26].

2.6 | Two-photon laser scanning microscopy

Isolated pial arteries (E1-E4) with an average length of 2–3 mm were mounted between two glass micropipettes (100–125 μm) of an arteriography organ chamber (Living Systems Instrumentation, Burlington, VT). After flushing residual luminal blood out, the arterial vascular wall was visualized with TPLSM, using a Leica TCS SP5 (Leica Microsystems GmbH, Wetzlar, Germany). A Ti:Sapphire Chameleon Ultra II (Coherent) mode locked at 820 nm was used as the excitation source. A Leica HCX APO L ×20/1.00 objective was used for excitation and epi-collection. Three color-coded channels were used for detection, namely 399–499 nm (blue, for detection of adventitial collagen using second harmonic generation microscopy), 509–552 nm (green, for detection of lipofuscin and intraluminal fluorescein isothiocynate [FITC-]dextran), and 568–650 nm (red, for detection of lipofuscin).

Thereafter, TPLSM image stacks were included for quantitative analysis of the autofluorescent particles. Quantification was performed with Imaris© image-processing software (Imaris, RRID:SCR_007370, version 8.3, Bitplane AG, Zürich) providing a 3D reconstruction of the stacks. Using this technique, sampling errors due to possible heterogenous distribution of autofluorescent particles are avoided, in contrast to quantification of autofluorescent particles on tissue sections. Furthermore, the 3D representations allow spatial visualization of particle distribution and density, as well as assessment of particle volume and shape.

Fluorescent particles were defined by their threshold, which was determined based on intensity in relation to background signal and local contrast. Optimal threshold levels were set separately for each stack, following inter-observer agreement of two independent observers [LO and DK]. Validation of the segmentation was performed by superimposing the reconstructed autofluorescent particles on the original confocal z-stack. Subsequently, the red channel was selected to calculate the number of particles, particle density, and diameter distribution. Finally, volume reconstruction was performed on the 3D image of the stack in the red channel to determine mean particle volume and particle volume density.

3 | RESULTS

3.1 | Fluorescence spectroscopic imaging

Autofluorescent particles on neocortical slides of patients and controls were found throughout neocortical parenchyma, as well as near or within parenchymal vessels (Figure 1a,b). These autofluorescent particles appeared to be clustered predominately around parenchymal vessels, especially within the adventitia of the parenchymal arterioles. However, at a ×100 magnification this finding was not conclusive (Figure 1b).

Independent of their localization and in all samples, specific particles show a broad and sloping emission spectrum between 460 and 720 nm on excitation, with a maximum at 580 to 600 nm (Figure 2). Autofluorescence spectra were similar in patients and controls. The spectrum measured on the paraffin slides did not differ from that in fresh-frozen slides (not shown).

At ×100 magnification, we zoomed in on a single blood vessel, while using the spectra of Figure 2 for unmixing. This confirmed that all particles indeed had a similar autofluorescence spectrum. Moreover, particles were more clearly distinguished from the (autofluorescent) blood vessel background using the unmixing procedure (Figure 3).

3.2 | Brightfield microscopy and histochemistry

The autofluorescent particles in the native slide could be matched with PAS-positive particles in the adjacent slide, appearing as pronounced pink-red colored particles (Figure 4).

3.3 | Fluorescence lifetime imaging

In the next step, fluorescence lifetime of an autofluorescent particle surrounding a parenchymal vessel was analyzed in one patient (E1). First, spectrum analysis was repeated with two-photon laser scanning microscopy to verify that particles with similar spectral properties were analyzed. Indeed, identical spectra were found (data not shown). The autofluorescence intensity profile on pulsed excitation showed a biexponential decay. A fast component (τ_1) at 0.527 ± 0.026 ns and a slow component (τ_2) at 2.60 ± 0.10 ns were noted with a relative amplitude of 87 ± 4.4% (α_1) and 13 ± 0.65% (α_2), respectively. Based on these values, a mean lifetime of 1.41 ± 0.070 ns was calculated.

Lifetime analysis of a particle observed throughout the neocortical tissue of the same patient showed similar results. A mean lifetime of 1.53 ± 0.076 ns was calculated for those particles, based on τ_1 at 0.530 ± 0.027 ns and τ_2 at 2.97 ± 0.15 ns, with a relative amplitude of 89 ± .5% (α_1) and 11 ± 0.55% (α_2), respectively.

3.4 | Quantification of autofluorescent particles in pial arteries

We then focused on determining the localization and quantification of the autofluorescent particles in 3D within the vessel wall. For this purpose, we applied 3D two-photon laser scanning and second harmonic generation microcopy. Excised pial arteries, either from controls or patients, were mounted and pressurized on a vessel chamber and subsequently imaged. An abundant number of autofluorescent particles

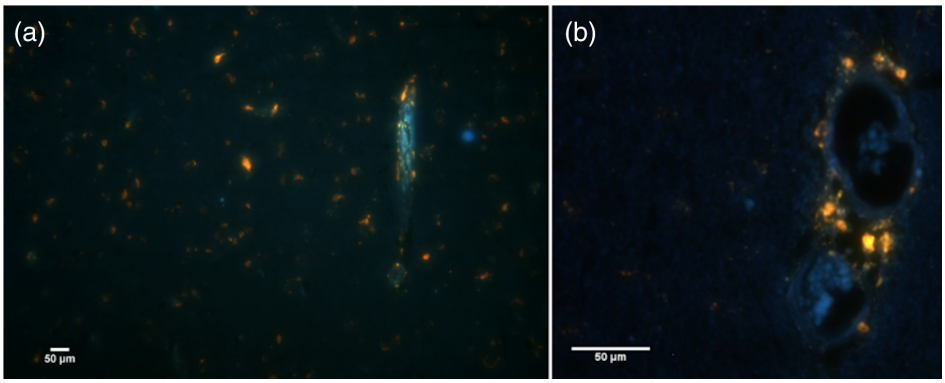

FIGURE 1 Autofluorescent particles in a neocortical sample of an epilepsy patient can be seen as yellowish bright dots. The blue-green autofluorescence of elastin in larger blood vessels is clearly visible. The particles are found throughout the neocortical; tissue (a), but seem strongly accumulating around and within parenchymal vessels (b). The vessels in image b seem to contain a small clot in their lumen. These images are derived using Nuance microscopy at a ×20 magnification [Color figure can be viewed at wileyonlinelibrary.com]

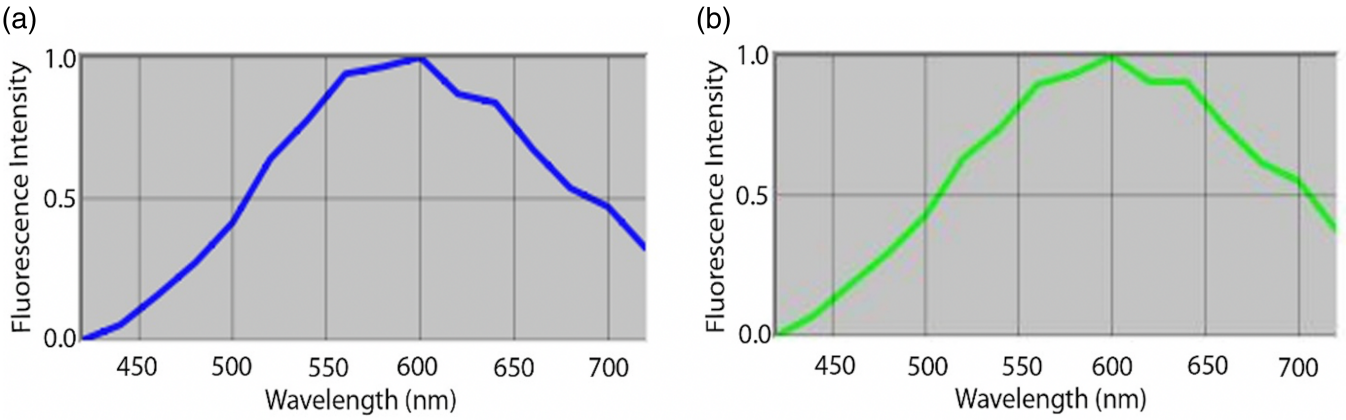

FIGURE 2 The emission spectra of the autofluorescent particles within the neocortical tissue slides of a patient (a) and a control (b) are illustrated. Emission wavelengths are found on the X-axis whereas the Y-axis represents fluorescence intensity of wavelength. A broad emission spectrum with a maximum intensity around 580 to 600 nm can be noted. A similar emission spectrum was found in representative particles of patient and control tissue. Emission spectra obtained using nuance microscopy at an excitation wavelength of 420–460 nm, using a long pass filter, passing emission wavelengths from 420 nm [Color figure can be viewed at wileyonlinelibrary.com]

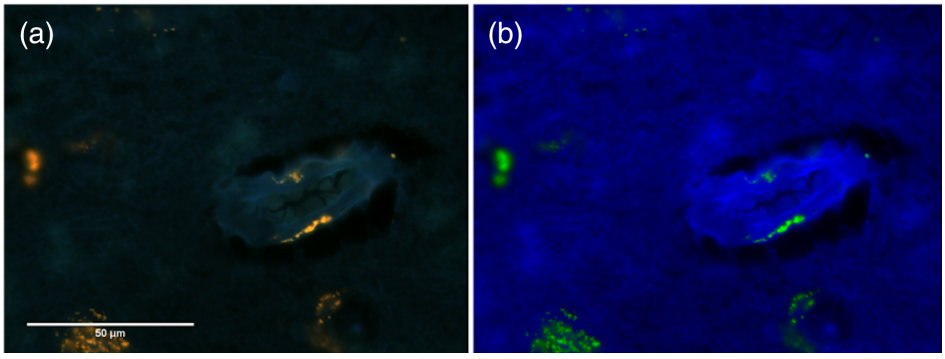

FIGURE 3 Autofluorescent yellowish particles within the wall of a parenchymal vessel, derived using nuance microscopy at ×100 magnification (a). Unmixed image (b). The lumen seems to contain a substance, probably a blood clot. Next, the endothelial cell layer is aligned by a brighter (pseudo-color) blueish layer, representing the internal elastic membrane. More outward in the vascular wall, the particles are noted. Hence, particles are most prominently located in the adventitia. As in Figure 4, particles are also found within the neocortical tissue, sometimes not surrounding a vascular lumen [Color figure can be viewed at wileyonlinelibrary.com]

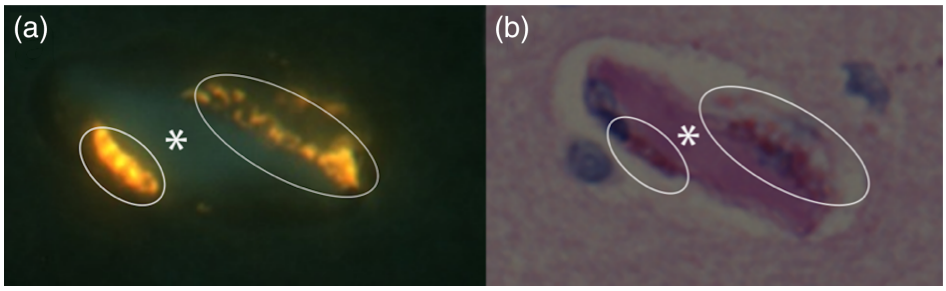

FIGURE 4 Autofluorescent (yellowish) particles (white ellipse) surrounding the lumen (white asterisk) of a parenchymal vessel can be noted when analyzed by Nuance microscopy at ×40 magnification (a). The 8 μm adjacent slide was stained using periodic acid Schiff's (b). Here, the autofluorescent particles are depicted as red-colored, PAS-positive, particles (white ellipse) surrounding the lumen (white asterisk) of the same parenchymal vessel [Color figure can be viewed at wileyonlinelibrary.com]

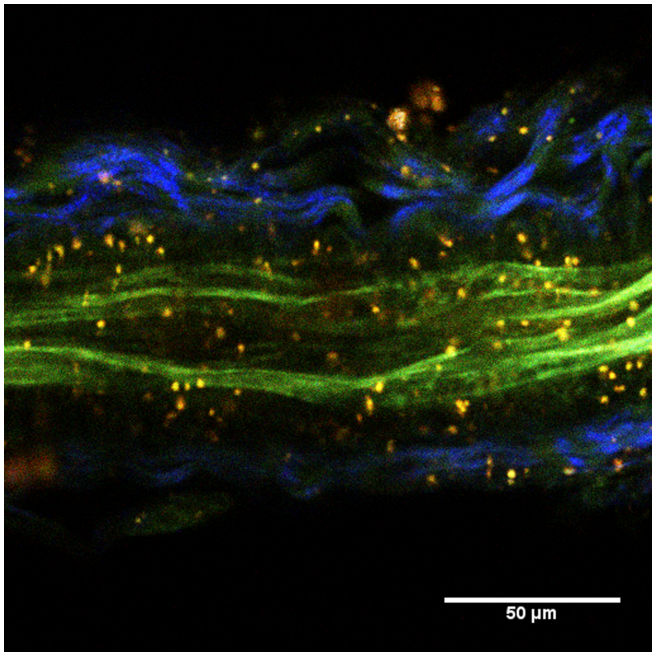

FIGURE 5 Autofluorescent particles appear as yellowish bright dots surrounding a pial artery, visualized with TPLSM (excitation wavelength: 820 nm). The green bands reflect autofluorescence of elastin within the internal elastic lamina. The blue wave-form strips on the upper and lower part of the vessels, that is, within the adventitia, reflect collagen as a result of second harmonic generation [Color figure can be viewed at wileyonlinelibrary.com]

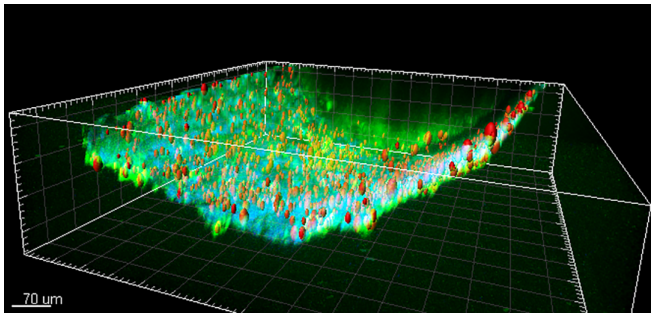

FIGURE 6 A representative spherical 3D-reconstruction of autofluorescent particles within a pial artery, in which lipofuscin particles are visualized as red-orange ellipses. The bright green glow is the result of fluorescence by intraluminal dextran-FITC (70kD) and autofluorescence of elastin within the inner elastic lamina (see also Figure 5). The light blue glow represent the wavy structures of adventitial collagen (see also Figure 5). Reconstruction based on Z-stack using TPLSM (excitation wavelength 820 nm) [Color figure can be viewed at wileyonlinelibrary.com]

was noted within isolated pial arteries of both groups (Figure 5). Image stacks of one patient (E1) were excluded due to poor image quality because of overexposure of excitation light.

A representative spherical 3D-reconstruction of particles in the vessel wall is shown in Figure 6. These reconstructions allowed localization of these particles within the pial artery, using Imaris© software. Here, the autofluorescent particles appeared to be surrounding the external elastic membrane and therefore appeared to be mainly located within the adventitia, and to a lesser extent in the tunica media. No particles were detected in the intima and lumen, as visualized by the clear delineation of dextran-FITC in the lumen. Results comparing patients and control with respect to mean particle diameter, volume and density are given in Table 2 and Figures 6 and 7.

4 | DISCUSSION

In this study, we have identified and described autofluorescent properties of lipofuscin particles within human cerebral tissue of epilepsy patients and controls. We have observed these particles within the brain parenchyma and within the cerebral vascular wall. This is the first report on cerebral lipofuscin accumulation within the cerebral vascular wall. Additionally, we have performed a robust and repeatable quantitative analysis of lipofuscin particles in 3D images.

4.1 | Autofluorescent properties of lipofuscin

In order to classify the autofluorescent particles as lipofuscin, we performed a number of consecutive experiments, beginning with

TABLE 2 Quantification analysis of autofluorescent particles within pial arteries

	E2	E3	E4	C1
Total vessel wall volume included (μm^3) • 10E6	94,39	2,13	0,64	8,70
Mean diameter per particle (μm)	4.81	3.11	2.78	4.79
Mean volume per particle (μm^3)	163	44	30	145
Density of particles in the vascular wall (number of particles/total stack volume) • 10E6	85	199	642	135
Volume density of particles in the vascular wall (%) (volume particles [μm^3]/total stack volume [μm^3]) • 100%	1.38	0.88	1.93	1.97

Note: Quantification analysis of autofluorescent particles within pial arteries for three epilepsy patients (E1, E2, E3) and one control (C1).

conventional light microscopy to examine PAS-stained sections. This revealed PAS-positive particles throughout the samples, but mainly within the vessel wall, and matching with the autofluorescent particles on adjacent section slides. PAS staining is not lipofuscin-specific, since it also stains glycogen and other polysaccharide containing substances. However, the match with the specific autofluorescent signal (see below) confirms that the particles indeed represent lipofuscin. Therefore, we performed no additional stainings for lipofuscin. In future studies, other non-lipofuscinspecific staining methods—like Sudan III-staining, Schmorl method I or silver impregnation combined with performic acid oxidation—could be considered for lipofuscin detection as well (Braak, Braak, Ohm, & Bohl, 1988; Marani, Usunoff, & Feirabend, 2009).

Then, we further characterized the autofluorescent properties of the particles. Fluorescence spectral analysis revealed a broad emission spectrum with a maximum between 580 and 600 nm. These results are comparable to spectral properties of lipofuscin described in literature (Berezin & Achilefu, 2011; Marmorstein, Marmorstein, Sakaguchi, & Hollyfield, 2002; Mochizuki, Park, Mori, & Kawashima, 1995; Schweitzer et al., 2007; Seehafer & Pearce, 2006; Sparrow & Boulton, 2005). Since lipofuscin encompasses a wide variety of lipopigments, the autofluorescence spectrum is broad and depends on the ratio of varying fluorescent lipopigmental constituents (Katz & Robison, 2002; Mochizuki et al., 1995). Consequently, spectral variations between different tissues, and possibly between different species, have been described, in addition to variations due to distinct detection methods (Mochizuki et al., 1995; Seehafer & Pearce, 2006; Yin & Brunk, 1991). Nevertheless, autofluorescence analysis has been regarded as a reliable method to assess the presence of lipofuscin, both qualitatively and quantitatively (Mochizuki et al., 1995).

A similar broad autofluorescence spectrum is also found in advanced glycation end-products (Chorvatova & Chorvat, 2015; Ramanujam, 2000). To distinguish these from lipofuscin, fluorescence lifetime analysis was performed. We have observed a fluorescence lifetime of 1.41 ± 0.070 ns to 1.53 ± 0.076 ns and compared this with two other available studies on lipofuscin lifetime analysis, both carried out in retinal tissue (Berezin & Achilefu, 2011; Schweitzer et al., 2007). The first study characterizes lipofuscin with a fast component (τ_1) at 0.390 ± 0.020 ns, a slow component (τ_2) at 2.24 ± 0.11 ns, and a mean lifetime of 1.98 ± 0.10 ns based on associated relative amplitudes α_1 of 48 ± 2.4% and α_2 at 52 ± 2.6% (Schweitzer et al., 2007). In the same study, advanced glycation end products exhibit a bi-exponential decay with a fast component (τ_1) at 0.865 ± 0.43 ns and a slow component (τ_2) at 4.17 ± 0.20 ns, with a relative amplitude of 62 (α_1) ± 3.1% and 28 (α_2) ± 2.2%, respectively, resulting in a mean lifetime (τ_{mean}) of 3.13 ± 0.18 ns (Schweitzer et al., 2007). In the other study, a mean lifetime of 1.34 ± 0.067 ns for lipofuscin is reported, without description of the calculation method used (Berezin & Achilefu, 2011). The mean fluorescence lifetime we found is comparable to the other two reported values on lipofuscin lifetime. Hence, we conclude that the autofluorescent particles detected are indeed lipofuscin.

4.2 | Quantification of lipofuscin

Previously published papers on lipofuscin accumulation were mostly qualitative and semi-quantitative using fluorescence microscopy or confocal laser scanning microscopy. These studies indeed demonstrated an age-related lipofuscin increase (Benavides, Monserrat, Fariña, & Porta, 2002; Brizzee, Ordy, & Kaack, 1974; Jung et al., 2010; Nakae & Stoward, 2016; Tohma et al., 2011). Quantification methods relied on 2D counting using fluorescence microscopy or confocal laser scanning microscopy on histological slides. Such 2D methods are semi-quantitative, because they are prone to subjective assessment, and limited regarding precision and sensitivity, by factors such as magnification, tissue thickness, and tissue level. To improve quantification, threshold based analysis has been proposed and statistical analysis was added for a more objective estimation (Tohma et al., 2011). However, accurate quantification requires a 3D approach, because it overcomes 2D-related impeding factors including tissue thickness (Douma et al., 2010).

We therefore subsequently performed a 3D quantitative analysis of the particles within the pial arterial wall in three patients and one control, using Imaris© software. For this analysis, we have used the TPLSM Z-stack image files.

This way, particle diameter, particle volume, and total vessel wall volume were determined, and particle and volume density were calculated (Table 2 and Figure 7). Regarding mean particle diameter and volume, we found that mean diameter of a particle is not proportionally related to its mean volume. This suggests that lipofuscin particles are not spherical, but have a complex 3D configuration. Additional volume reconstruction indeed confirmed this complex shape.

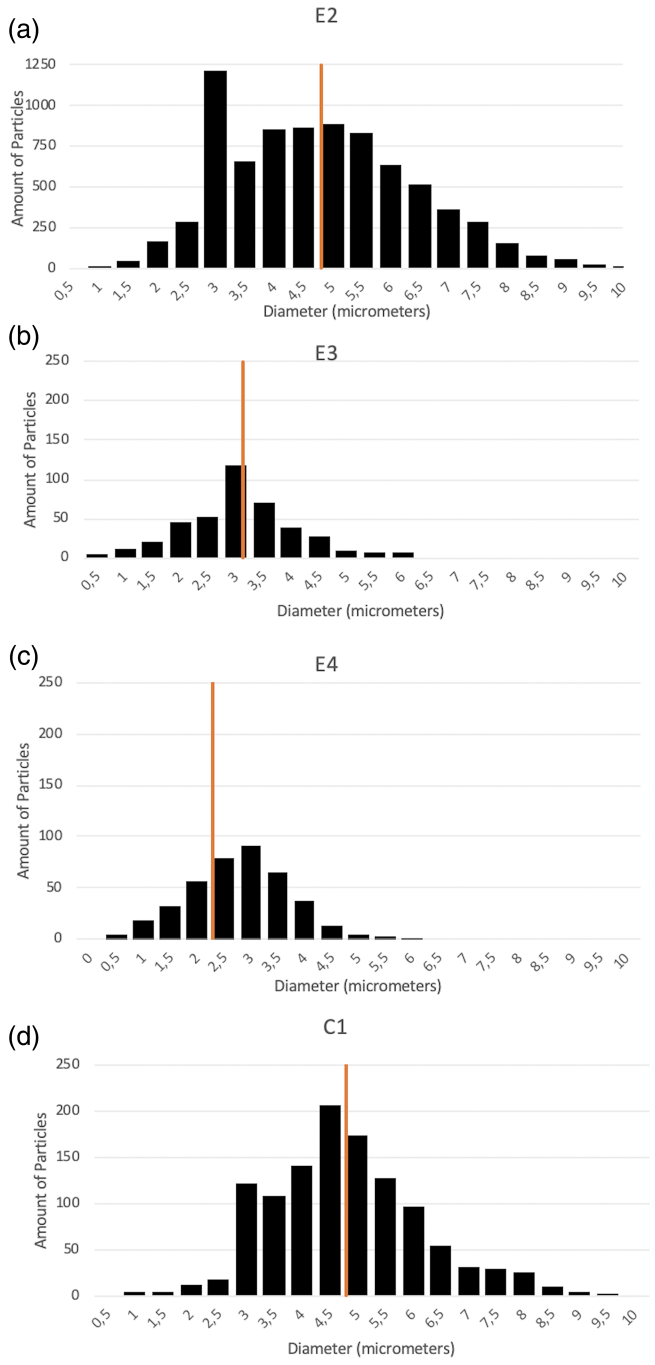

FIGURE 7 Diameters distribution of the autofluorescent particles within the pial artery wall of three patients (a, b, c) and one control (d). For each diameter, we have calculated the total number of particles within the image stack obtained with TPLSM. Since the image stack of E2 (a) was evidently larger than the other image stacks, a 10-fold larger number of particles per vessel was noted in this patient. Most particles were found to have a diameter between 2 and 6 μm. The red vertical line shows the mean diameter [Color figure can be viewed at wileyonlinelibrary.com]

The volume estimations in a 3D reconstruction approach as described here, thus offer an advantage over quantification methods on histological slides as described previously (Douma et al., 2010). In addition, quantification on tissue sections was previously hindered by heterogeneous distribution of fluorescent granules, demanding analysis of images of subsequent histological slices. This can give significantly deviating results (Douma et al., 2010) and it increases workload significantly (Douma et al., 2010; Fonseca, Sheehy, Blackman, Shelton, & Prior, 2005; Nakano & Gotoh, 1992; Tohma et al., 2011). Automated quantification with Imaris© complements TPLSM in analyzing multiple images, thereby increasing the precision of estimations. The software additionally provides spatial information, enables measurement of structures and offers more accurate localization than 2D methods. The spatial visualization rendering is an advantage of Imaris© over (semi)automated software packages that stepped in on the need for more precise quantification methods.

It should be noted that images of patient E2 included six Z-stack files, whereas all other image files included one Z-stack file. As a consequence, total vessel wall volume of E2 is much larger. To avoid sampling bias, we took the mean of all z-stacks for E2, instead of selecting one z-stack for comparison. Nonetheless, it is possible that by including multiple z-stacks, an overlap of vessel surface could have been considered in the calculation. This could result in an overestimation of the amount of particles present.

4.3 | Age and disease-related formation of lipofuscin

A gradual accumulation of lipofuscin within neuronal tissue during aging has previously been described in neuroscientific literature (Benavides et al., 2002). This is the first report that also demonstrates lipofuscin accumulation within the cerebral vascular wall. Our sample size is too small to look for group differences. Furthermore, the two groups are not age-matched which makes it impossible to attribute potential changes to either age or disease. However, we did a number of remarkable observations that we want to highlight here.

Lipofuscin particle density was 1.5 to 4.8 times higher in two young (18 and 28 years old) patients compared to the control (61 years old), suggesting a disease-related increase in lipofuscin formation.

Lipofuscin particle size varied amongst patients: two patients (E3 and E4) had small particles compared to control, while one patient (E2) had similarly sized particles. One could hypothesize that smaller particles are related to brief periods of oxidative stress (e.g., during seizures), whereas larger particles are the results of sustained oxidative stress (e.g., during normal aging). This might result in the larger number of smaller sized particles in patients. However, oxidative stress resulting in structural cell damage is in itself an intricate process (Czerska et al., 2015; Lushchak, 2014; Sies, 1997).

Lipofuscin formation within the cerebral vascular wall may be a "physiological" finding since we found lipofuscin particles in control tissue as well. Even though we cannot draw conclusions based on the small groups analyzed in our study, there may be a relation between shape, size, and density of lipofuscin and the epileptic seizures, that are associated with extreme and rapidly changing hemodynamic conditions, and structural and functional vascular abnormalities (Helakari et al., 2019; Patel, Zhao, Ma, & Schwartz, 2013).

4.4 | Clinical significance of this study

The pathophysiology of several neurological diseases like Alzheimer's disease, Parkinson's disease, and epilepsy has been related to oxidative stress (Islam, 2017; Pearson-Smith & Patel, 2017). These diseases seem to share a pathophysiological pathway, including microvascular dysfunction, increased blood–brain barrier permeability, angiogenesis, and dysfunctional neurovascular coupling (Brown & Thore, 2011; Erdő, Denes, & de Lange, 2016; Heinemann et al., 2012; Iadecola, 2004; Marchi & Lerner-Natoli, 2013; Parfenova et al., 2005; Rigau et al., 2007; E. van Vliet, Aronica, & Gorter, 2014). Hence, these diseases may be characterized by lipofuscin accumulation within the brain and the brain's vascular structures. Better understanding of the pathophysiology of these neurological diseases may thus come from better understanding the process of lipofuscin accumulation.

4.5 | Lipofuscin as a marker for oxidative stress

Since oxidative stress is a key process underlying the various mechanisms and pathways leading to lipofuscin formation, the demonstration of lipofuscin could be a novel method to assess the history of oxidative stress. However, it must be noted that alterations in various cellular pathway are recognized to contribute to the formation of lipofuscin. The finding of lipofuscin does not disclose the precise underlying mechanism responsible for its own formation. Hence, it is of importance to verify the relation with oxidative stress as we suggest.

Currently, assessment and quantification of oxidative stress is challenging. The amount of oxidative stress can be estimated by evaluation of reactive oxygen species. However, this method is difficult and unreliable since reactive oxygen species are transient and highly unstable. Therefore, mainly indirect markers for oxidative stress are used, which include lipid and protein oxidation such as 4-hydroxy-2-nonenal (4-HNE), malondialdehyde (MDA), and isoprostanes (e.g., 8-iso-$PGF_{2\alpha}$). Although these biomarkers have been analyzed thoroughly, interpretation is difficult due to a wide variation of detection methods (e.g., mass-spectometry, spectrophotometry, or immunodetection-based), sampling methods, and types of tissue/species assessed, leading to a broad range of reference intervals (Tsikas, 2017; Waldbaum & Patel, 2010). Moreover, assessment of some biomarkers is prone to many analytical pitfalls. For example, MDA levels are easily disturbed by sampling methods, sample storage, and artefactual formation (Tsikas, 2017). The analysis of 4-HNE is also complicated due its strong reactivity, in particular with certain proteins, forming HNE adducts (Spickett, 2013; Wakita, Honda, Shibata, Akagawa, & Uchida, 2011). Consequently, detection methods of free 4-HNE or its adducts are lacking accuracy and specificity, and—when reliable—analyses are time-consuming and laborious (Spickett, 2013; Wakita et al., 2011). Chemical lipid peroxidation leads to synthesis of 8-iso-$PGF_{2\alpha}$, which is often considered the gold standard for lipid peroxidation analysis (Van 't Erve et al., 2015). However, inflammation-induced *enzymatic* lipid peroxidation also results in biosynthesis of 8-iso-$PGF_{2\alpha}$, making it difficult to differentiate between ongoing inflammation or oxidative stress. Despite the limitations of these biomarkers, their analysis in adjunct to lipofuscin assessment could further substantiate the suggested relation between lipofuscin and oxidative stress.

Lipofuscin is a stable marker due to its nondegradable nature. This enables assessment in various tissue samples, not only in fresh-frozen tissue, but also in paraffin-fixed postmortem tissue. Using 3D TPLSM combined with dedicated image processing software, we have shown here that reliable quantification is enabled and subsequent particle size and density characteristics can easily be assessed. As such, lipofuscin could function as a marker of the total amount of oxidative stress endured by the tissue, during aging and the course of neurological diseases.

4.6 | Limitations of this study

The major limitations of this study include the small sample size and the lack of age-matched controls. Since it is difficult to obtain healthy brain tissue during resective brain surgery, we relied on postmortem tissue of people that died of a non-neurological cause. The age of these postmortem controls is therefore considerably higher than the age of epilepsy patients undergoing resective brain surgery.

4.7 | Future perspectives

Further understanding of the cellular pathways involved in the formation of lipofuscin is an important topic, that might foster our understanding of the pathophysiology of neurological diseases in relation to lipofuscin formation. In this regard, we believe that relating lipofuscin formation to oxidative stress by comparing it to biomarkers of oxidative stress is an interesting first aim. Future studies that assess lipofuscin accumulation in epilepsy patients compared to controls, for example, postmortem tissue of people that died of non-neurological cause, can provide important insights into the pathophysiology of epilepsy. The role of lipofuscin accumulation within the vascular wall, in addition to lipofuscin-accumulation in post-mitotic cells such as neurons, should be further studied. Additionally, it might be interesting to look at lipofuscin accumulation in and around other, more approachable vessels. A possible link between this and for example pial arteries then might result in the possibility to translate this method to patients in early stages of disease.

5 | CONCLUSIONS

Lipofuscin is present in the brain's pial arterial wall and neocortical parenchyma in young epilepsy patients and aged controls. A robust evaluation of the particles using Imaris© software allows robust quantification of the particles, while the 3D properties allow visualization of the complex configuration. Analysis of lipofuscin could be a new method to detect and quantify oxidative stress. Further research on

lipofuscin in relation to neurological diseases and oxidative stress, and to normal aging is warranted.

CONFLICT OF INTEREST

The authors declare no potential conflict of interest.

PEER REVIEW

The peer review history for this article is available at https://publons.com/publon/10.1002/cne.24971.

DATA AVAILABILITY STATEMENT

Raw data were generated at Maastricht University Medical Center. Derived data supporting the findings of this study are available from the corresponding author KH on request.

ORCID

Karlijn Hakvoort https://orcid.org/0000-0001-6822-130X

REFERENCES

Aguiar, C. C. T., Almeida, A. B., Arajo, P. V. P., De Abreu, R. N. D. C., Chaves, E. M. C., Do Vale, O. C., … M, S. M. (2012). Oxidative stress and epilepsy: Literature review. *Oxidative Medicine and Cellular Longevity*, *2012*, 1–12. https://doi.org/10.1155/2012/795259

Benavides, S. H., Monserrat, A. J., Fariña, S., & Porta, E. A. (2002). Sequential histochemical studies of neuronal lipofuscin in human cerebral cortex from the first to the ninth decade of life. *Archives of Gerontology and Geriatrics*, *34*(3), 219–231. https://doi.org/10.1016/S0167-4943(01)00223-0

Berezin, M. Y., & Achilefu, S. (2011). Fluorescence lifetime measurements and biological imaging. *Chemical Reviews*, *110*(5), 2641–2684. https://doi.org/10.1021/cr900343z.Fluorescence

Braak, H., Braak, E., Ohm, T., & Bohl, J. (1988). Silver impregnation of Alzheimer's neurofibrillary changes counterstained for basophilic material and lipofuscin pigment. *Stain Technology*, *63*(4), 197–200. https://doi.org/10.3109/10520298809107184

Brizzee, K. R., Ordy, J. M., & Kaack, B. (1974). Early appearance and regional differences in intraneuronal and extraneuronal lipofuscin accumulation with age in the brain of a nonhuman primate (*Macaca mulatta*). *Journals of Gerontology*, *29*(4), 366–381. https://doi.org/10.1093/geronj/29.4.366

Brown, W. R., & Thore, C. R. (2011). Review: Cerebral microvascular pathology in aging and neurodegeneration. *Neuropathology and Applied Neurobiology*, *37*(1), 56–74. https://doi.org/10.1111/j.1365-2990.2010.01139.x.Review

Brunk, U. T., & Terman, A. (2002). The mitochondrial-lysosomal axis theory of aging: Accumulation of damaged mitochondria as a result of imperfect autophagocytosis. *European Journal of Biochemistry*, *269*(8), 1996–2002. https://doi.org/10.1046/j.1432-1033.2002.02869.x

Chang, S. J., & Yu, B. C. (2010). Mitochondrial matters of the brain: Mitochondrial dysfunction and oxidative status in epilepsy. *Journal of Bioenergetics and Biomembranes*, *42*(6), 457–459. https://doi.org/10.1007/s10863-010-9317-4

Chorvatova, A., & Chorvat, D. (2015). Tissue fluorophores and their spectroscopic characteristics. In L. Marcu, P. French, & D. Elson (Eds.), *Fluorescence lifetime spectroscopy and imaging: Principles and applications in biomedical diagnostics* (pp. 47–76). Taylor & Francis Group: CRC Press.

Collins, V., Arborgh, B., Brunk, U., & Schellens, J. (1980). Phagocytosis and degradation of rat liver mitochondria by cultivated human glial cells. *Laboratory Investigation*, *42*(2), 209–2016.

Czerska, M., Mikołajewska, K., Zieliński, M., Gromadzińska, J., & Wąsowicz, W. (2015). Today's oxidative stress markers. *Medycyna Pracy*, *66*(3), 393–405. https://doi.org/10.13075/mp.5893.00137

Douma, K., Oostendorp, M., Slaaf, D. W., Post, M. J., Backes, W. H., & Van Zandvoort, M. A. M. J. (2010). Evaluation of magnetic resonance vessel size imaging by two-photon laser scanning microscopy. *Magnetic Resonance in Medicine*, *63*(4), 930–939. https://doi.org/10.1002/mrm.22248

Erdő, F., Denes, L., & de Lange, E. (2016). Age-associated physiological and pathological changes at the blood–brain barrier: A review. *Journal of Cerebral Blood Flow & Metabolism*, *37*(1). https://doi.org/10.1177/0271678X16679420, 4, 24

Fonseca, D. B., Sheehy, M. R. J., Blackman, N., Shelton, P. M. J., & Prior, a. E. (2005). Reversal of a hallmark of brain ageing: Lipofuscin accumulation. *Neurobiology of Aging*, *26*(1), 69–76. https://doi.org/10.1016/j.neurobiolaging.2004.02.013

Heinemann, U., Kaufer, D., & Friedman, A. (2012). Blood brain barrier dysfunction, TGFb signaling and astrocyte dysfunction in epilepsy. *Glia*, *60*(8), 1251–1257. https://doi.org/10.1002/glia.22311

Helakari, H., Kananen, J., Huotari, N., Raitamaa, L., Tuovinen, T., Borchardt, V., … Ansakorpi, H. (2019). Spectral entropy indicates electrophysiological and hemodynamic changes in drug-resistant epilepsy – A multimodal MREG study. *NeuroImage: Clinical*, *22*(March), 101763. https://doi.org/10.1016/j.nicl.2019.101763

Iadecola, C. (2004). Neurovascular regulation in the normal brain and in Alzheimer's disease. *Nature Reviews. Neuroscience*, *5*(5), 347–360. https://doi.org/10.1038/nrn1387

Islam, M. T. (2017). Oxidative stress and mitochondrial dysfunction-linked neurodegenerative disorders. *Neurological Research*, *39*(1), 73–82. https://doi.org/10.1080/01616412.2016.1251711

Jung, T., Höhn, A., & Grune, T. (2010). Lipofuscin: Detection and quantification by microscopic techniques. *Methods in Molecular Biology*, *594*, 173–193. https://doi.org/10.1007/978-1-60761-411-1_13

Katz, M. L., & Robison, W. G. (2002). What is lipofuscin? Defining characteristics and differentiation from other autofluorescent lysosomal storage bodies. *Archives of Gerontology and Geriatrics*, *34*(3), 169–184. https://doi.org/10.1016/S0167-4943(02)00005-5

Lin, M. T., & Beal, M. F. (2006). Mitochondrial dysfunction and oxidative stress in neurodegenerative diseases. *Nature*, *443*(7113), 787–795. https://doi.org/10.1038/nature05292

Lushchak, V. I. (2014). Free radicals, reactive oxygen species, oxidative stress and its classification. *Chemico-Biological Interactions*, *224*, 164–175. https://doi.org/10.1016/j.cbi.2014.10.016

Marani, E., Usunoff, K. G., & Feirabend, H. K. P. (2009). Lipofuscin and Lipofuscinosis. In L. R. Squire (Ed.), *Encyclopedia of Neuroscience* (pp. 481–486). Academic Press. https://doi.org/10.1016/B978-008045046-9.00126-1

Marchi, N., Betto, G., Fazio, V., Fan, Q., Ghosh, C., MacHado, A., & Janigro, D. (2009). Blood-brain barrier damage and brain penetration of antiepileptic drugs: Role of serum proteins and brain edema. *Epilepsia*, *50*(4), 664–677. https://doi.org/10.1111/j.1528-1167.2008.01989.x

Marchi, N., & Lerner-Natoli, M. (2013). Cerebrovascular remodeling and epilepsy. *The Neuroscientist*, *19*(3), 304–312. https://doi.org/10.1177/1073858412462747.Cerebrovascular

Marmorstein, A. D., Marmorstein, L. Y., Sakaguchi, H., & Hollyfield, J. G. (2002). Spectral profiling of autofluorescence associated with lipofuscin, Bruch's membrane, and sub-RPE deposits in normal and AMD eyes. *Investigative Ophthalmology and Visual Science*, *43*(7), 2435–2441.

Mochizuki, Y., Park, M. K., Mori, T., & Kawashima, S. (1995). The difference in autofluorescence features of lipofuscin between brain and adrenal. *Zoological Science*, *12*, 283–288. https://doi.org/10.2108/zsj.12.283

Moreno-García, A., Kun, A., Calero, O., Medina, M., & Calero, M. (2018). An overview of the role of lipofuscin in age-related neurodegeneration. *Frontiers in Neuroscience*, *12*(464), 1–13. https://doi.org/10.3389/fnins.2018.00464

Nakae, Y., & Stoward, P. J. (2016). The high correlation between counts and area fractions of lipofuscin granules, a biomarker of oxidative stress in muscular dystrophies. *Histochemistry and Cell Biology*, *146*(5), 1–8. https://doi.org/10.1007/s00418-016-1462-3

Nakano, M., & Gotoh, S. (1992). Accumulation of cardiac lipofuscin depends on metabolic rate of mammals. *Journal of Gerontology*, *47*(4), B126–B129.

Parfenova, H., Carratu, P., Tcheranova, D., Fedinec, A., Pourcyrous, M., & Leffler, C. W. (2005). Epileptic seizures cause extended postictal cerebral vascular dysfunction that is prevented by HO-1 overexpression. *American Journal of Physiology. Heart and Circulatory Physiology*, *288*, H2843–H2850. https://doi.org/10.1152/ajpheart.01274.2004

Patel, K. S., Zhao, M., Ma, H., & Schwartz, T. H. (2013). Imaging preictal hemodynamic changes in neocortical epilepsy. *Neurosurgical Focus*, *34*(4), E10. https://doi.org/10.3171/2013.1.focus12408

Pauletti, A., Terrone, G., Shekh-ahmad, T., Salamone, A., Ravizza, T., Rizzi, M., … Vezzani, A. (2019). Targeting oxidative stress improves disease outcomes in a rat model of acquired epilepsy. *Brain*, *142*, 1–15. https://doi.org/10.1093/brain/awz092

Pearson-Smith, J. N., & Patel, M. (2017). Metabolic dysfunction and oxidative stress in epilepsy. *International Journal of Molecular Sciences*, *18*(11), 1–13. https://doi.org/10.3390/ijms18112365

Puttachary, S., Sharma, S., Stark, S., & Thippeswamy, T. (2015). Seizure-induced oxidative stress in temporal lobe epilepsy. *BioMed Research International.*, *2015*, 1–20. https://doi.org/10.1155/2015/745613

Ramanujam, N. (2000). Fluorescence spectroscopy in vivo. In R. A. Meyers (Ed.), *Encyclopedia of Analytical Chemistry* (pp. 20–56). Chichester: John Wiley & Sons Ltd. https://doi.org/10.1002/9780470027318.a0102.pub2

Rigau, V., Morin, M., Rousset, M.-C., de Bock, F., Lebrun, A., Coubes, P., … Lerner-Natoli, M. (2007). Angiogenesis is associated with blood-brain barrier permeability in temporal lobe epilepsy. *Brain*, *130*, 1942–1956. https://doi.org/10.1093/brain/awm118

Rumià, J., Marmol, F., Sanchez, J., Giménez-Crouseilles, J., Carreño, M., Bargalló, N., … Puig-Parellada, P. (2013). Oxidative stress markers in the neocortex of drug-resistant epilepsy patients submitted to epilepsy surgery. *Epilepsy Research*, *107*(1–2), 75–81. https://doi.org/10.1016/j.eplepsyres.2013.08.020

Schweitzer, D., Schenke, S., Hammer, M., Schweitzer, F., Jentsch, S., Birckner, E., … Bergmann, A. (2007). Towards metabolic mapping of the human retina. *Microscopy Research and Technique*, *70*, 410–419.

Seehafer, S. S., & Pearce, D. A. (2006). You say lipofuscin, we say ceroid: Defining autofluorescent storage material. *Neurobiology of Aging*, *27*(4), 576–588. https://doi.org/10.1016/j.neurobiolaging.2005.12.006

Sies, H. (1997). Oxidative stress: Oxidants and antioxidants. *Experimental Physiology*, *82*(2), 291–295. https://doi.org/10.1113/expphysiol.1997.sp004024

Sparrow, J. R., & Boulton, M. (2005). RPE lipofuscin and its role in retinal pathobiology. *Experimental Eye Research*, *80*(5), 595–606. https://doi.org/10.1016/j.exer.2005.01.007

Spickett, C. M. (2013). The lipid peroxidation product 4-hydroxy-2-nonenal: Advances in chemistry and analysis. *Redox Biology*, *1*(1), 145–152. https://doi.org/10.1016/j.redox.2013.01.007

Strehler, B. L., Mark, D. D., Mildvan, A. S., & Gee, M. V. (1959). Rate and magnitude of age pigment accumulation in the human myocardium. *Journal of Gerontology*, *14*(4), 430–439. https://doi.org/10.1093/geronj/14.4.430

Terman, A., & Brunk, U. T. (1998). Lipofuscin: Mechanisms of formation and increase with age. *APMIS: Acta Pathologica, Microbiologica, et Immunologica Scandinavica*, *106*(2), 265–276.

Terman, A., & Brunk, U. T. (2004). Lipofuscin. *The International Journal of Biochemistry & Cell Biology*, *36*(8), 1400–1404. https://doi.org/10.1016/j.biocel.2003.08.009

Tohma, H., Hepworth, A. R., Shavlakadze, T., Grounds, M. D., & Arthur, P. G. (2011). Quantification of ceroid and lipofuscin in skeletal muscle. *The Journal of Histochemistry and Cytochemistry: Official Journal of the Histochemistry Society*, *59*(8), 769–779. https://doi.org/10.1369/0022155411412185

Tsikas, D. (2017). Assessment of lipid peroxidation by measuring malondialdehyde (MDA) and relatives in biological samples: Analytical and biological challenges. *Analytical Biochemistry*, *524*, 13–30. https://doi.org/10.1016/j.ab.2016.10.021

Uttarra, B., Singh, A. V., Zamboni, P., & Mahajan, R. T. (2009). Oxidative stress and neurodegenerative diseases: A review of upstream and downstream antioxidant therapeutic options. *Current Neuropharmacology*, *7*, 65–74. https://doi.org/10.2174/157015909787602823

Van 't Erve, T. J., Lih, F. B., Kadiiska, M. B., Deterding, L. J., Eling, T. E., & Mason, R. P. (2015). Reinterpreting the best biomarker of oxidative stress: The 8-iso-PGF2α/PGF2α ratio distinguishes chemical from enzymatic lipid peroxidation. *Free Radical Biology and Medicine*, *83*, 245–251. https://doi.org/10.1016/j.freeradbiomed.2015.03.004

van Vliet, E., Aronica, E., & Gorter, J. (2014). Role of blood-brain barrier in temporal lobe epilepsy and pharmacoresistance. *Neuroscience*, *277*, 455–473. https://doi.org/10.1016/j.neuroscience.2014.07.030

van Vliet, E. A., Aronica, E., & Gorter, J. A. (2015). Blood–brain barrier dysfunction, seizures and epilepsy. *Seminars in Cell & Developmental Biology*, *38*, 26–34. https://doi.org/10.1016/j.semcdb.2014.10.003

Wakita, C., Honda, K., Shibata, T., Akagawa, M., & Uchida, K. (2011). A method for detection of 4-hydroxy-2-nonenal adducts in proteins. *Free Radical Biology and Medicine*, *51*(1), 1–4. https://doi.org/10.1016/j.freeradbiomed.2011.02.037

Waldbaum, S., & Patel, M. (2010). Mitochondria, oxidative stress, and temporal lobe epilepsy. *Epilepsy Research*, *88*, 23–45. https://doi.org/10.1016/j.eplepsyres.2009.09.020

Yin, D., & Brunk, U. T. (1991). Microfluorometric and fluorometric lipofuscin spectral discrepancies: A concentration-dependent metachromatic effect? *Mechanisms of Ageing and Development*, *59*(1–2), 95–109.

How to cite this article: Hakvoort K, Otto L, Haeren R, et al. Shedding light on human cerebral lipofuscin: An explorative study on identification and quantification. *J Comp Neurol*. 2021;529:605–615. https://doi.org/10.1002/cne.24971